Chapter 2
Quantitative Characterization of Lunar Mare Orientale Basalts Detected by Moon Mineralogical Mapper on Chandrayaan-1

S. Arivazhagan

Abstract Efficient lunar resource utilization requires accurate and quantitative evaluation of mineral and glass abundances, distribution, and extraction feasibility, especially for ilmenite (TiO_2). The modal analyses have performed on lunar basaltic terrains using hyperspectral remote sensing data along with ground truth chemistry and mineralogy. The main aim of the present work is to characterize the lunar Mare Orientale basalts based on TiO_2 content and quantify the lunar surface minerals, including clinopyroxene, orthopyroxene, plagioclase, and olivine. The Orientale basin is one of the youngest impact multi-ringed basins on the Moon covering 930 km in diameter centered at 20°S 95°W. The morphological features in the Orientale basin have developed interest among geoscientist to explore further study on this region. Based on the Apollo orbital, geochemical, and Earth-based spectral data, it is concluded that the Orientale ejecta are uniformly feldspathic in composition, almost pure anorthosite with no evidence of ultramafic components (Hawke, Geophys Res Lett 18(11):2141–2144, 1991). Greeley et al. (Geophys Res 98:17183–17205, 1993) have conferred the Orientale basin bearing the low-Ti basalts by using Galileo images. In this study, parts of basaltic regions of Mare Orientale, Lacus Veris, and Lacus Autumni of the Orientale basin are investigated using Moon Mineralogical Mapper (M^3) data of onboard Chandrayaan-1 orbiter. Lucey's (1998) TiO_2 estimation method and spectral profiles and spectral unmixing techniques have been used to detect and map the minerals, including plagioclase, clinopyroxene, orthopyroxenes, olivine, and various basalts such as low-, medium-, and high-Ti basalts. The Orientale data were acquired by M^3's reduced resolution mode with 20–40 nm spectral resolution and 140 m/pixel across the 40 km field of view. The RELAB mineral spectra of plagioclase, clino/orthopyroxenes, olivine and

S. Arivazhagan (✉)
Department of Geology, Periyar University, Salem 636 011, Tamil Nadu, India

Department of Civil Engineering, KSR College of Engineering, Tiruchengode 637215, Tamil Nadu, India
e-mail: arivusv@gmail.com

S. Jin et al. (eds.), *Planetary Exploration and Science: Recent Results and Advances*, Springer Geophysics, DOI 10.1007/978-3-662-45052-9_2

various basaltic spectra, chemistry and mineralogy have been employed to unmixing analysis. Comparing the spectral profiles of the basaltic regions with the RELAB basaltic spectra, the distribution and nature of TiO_2 basalts in the Orientale basaltic regions have been analyzed in quantitative manner in the present research.

Keywords Mare Orientale • Lacus Veris • Lacus Autumni • Spectral unmixing • End-member

2.1 Introduction

The lunar mare basalts are concentrated on the near surface of the Moon. The low-albedo smooth plains of lunar mare basalt covered almost 20 % of the lunar surface (Head 1976). Right from the beginning of lunar observation, the distinction between the lunar highlands and maria has been recognized (Taylor 1975). The 16 % of the lunar surface is covered by about 23 lunar mares, most of which are located in the near side of the Moon and the remaining three mares such as Mare Orientale, Mare Moscoviense and Mare Ingenii are located in the far side of the Moon. The lunar rock samples collected through Apollo and "Luna" series missions indicated that the lunar mare materials are predominantly composed of basalts. The lunar surface is mainly composed of plagioclase, pyroxene, olivine, ilmenite, agglutinitic and volcanic glass. The mineralogical diversity of the mare basalts has been examined through spectroscopy and linked to the surface units of returned samples (Pieters 1978, 1993; Staid et al. 1996; Staid 2000; Lucey et al. 2006).

The major minerals among various types of mare basalt are pyroxene, Mg-rich olivine, Ca-rich feldspar, and ilmenite (McCord et al. 1972). Lunar basalt samples approximately consist of 51 % of pyroxene, 27 % plagioclase, 8 % olivine and 11 % opaques (Crown and Pieters 1987). In general, the Fe- and Mg-rich mare regions contain abundant calcic pyroxenes and the Al-rich highlands contain low-calcium pyroxenes; both exhibit diagnostic absorption features in the reflectance spectral profile (Adams 1974). The dominant pyroxene in the mare basalt is high Ca-clinopyroxene. Titanium is one of the major elements in mare rocks and accounts for 0.5–13 %. Based on titanium content, the basalts can be divided into three types: high-Ti basalts, low-Ti basalts, and high-Al, low-Ti basalts (Cloutis and Gaffey 1991). Although a variety of distinct basalt types exist, pyroxene is the most abundant mineral in these basalts, followed by plagioclase. The amount of olivine and ilmenite in the basalts varies from minor to 20 % (Pieters and Englert 1997).

Hyperspectral remote sensing or imaging spectroscopy and reflectance spectroscopy are efficient tools to detect and quantify the mineral compositions on Earth and planetary surfaces (Shkuratov et al. 2007; Chen et al. 2007; Pieters et al. 2008; Clark et al. 2008). Nowadays, although mineral species could be successfully detected by hyperspectral data (Clark et al. 2003), the mineral abundance is difficult to retrieve. Retrieval of mineral abundance is hindered by the complexities of mixture characteristics of mineral spectra.

The mineral mapping of the lunar surface can be broadly subdivided into global and regional mineral mapping. The regional mineral mapping concentrates on some important locations of mare and highland region where the drastic mineral compositional changes exist (Staid and Pieters 2000; LeMouélic et al. 1999; LeMouélic and Langevin 2001; Pieters et al. 2001). The purpose of mineral mapping is efficient lunar resource utilization, which requires accurate and quantitative evaluation of mineral and glass abundances, distribution, and extraction feasibility, especially for ilmenite. Common rock-forming minerals exhibit wavelength-dependent spectral features throughout the VNIR (0.4–1.0 μm), SWIR (1.0–2.5 μm), and TIR (5–25 μm) wavelength ranges.

The linear spectral unmixing is an efficient tool to quantify the materials distributed in the image. The spectral unmixing tool is used to decompose a reflectance (or corrected radiance) source spectrum into a set of given end-member spectra. The result of the unmixing is a measure of the membership of the individual end-member to the source spectrum. Linear unmixing has proven to be the most efficient algorithm to separate spectral fingerprints in hyperspectral images, but it requires known reference for giving input to match the spectra called end-member spectra for all of the probes present in the image. In general terms, linear unmixing is currently the most powerful technique for matching the spectral variations and establishing the quantitative mapping. It is often the case in remote sensing, that one wants to deal with identification, detection, and quantification of fractions of the target materials for each pixel for diverse coverage in a region using unmixing approaches to discern the proportion of heterogeneity (Kanniah et al. 2001). Linear mixture modeling assumes that the signal received by the satellite sensor depends on the proportion of individual surface components during the mixing process, such as soil, water, and vegetation present in a particular pixel (Abdul 2003). The unmixing decomposes a mixed pixel into a collection of end-members and a set of fractional abundances that indicate the proportion of each end-member available in the images. The contribution of each pixel is assigned to the percentage of area each ground cover class occupies in the pixel (Boardman 1989).

2.2 Study Area

In the present study, the basaltic regions of the Orientale basins such as Mare Orientale South's central part centered at 21.3′S and 265.4′E, Lacus Veris' central part located at 14°S and 273°E, and the main portion of the Lacus Autumni centered at 12°S and 277.5′E test sites are selected for carrying out the analysis. The following criteria were taken in mind to select the Orientale basin as the study area; Mare Orientale (the "eastern sea") is one of the most striking lunar features on a large scale. Since the Orientale basin has not been sampled by the Apollo program, the basin's precise age is not known. Unlike most other basins on the Moon, Orientale is relatively less flooded by mare basalts and exposes much of the

basin structure to view. The Orientale basin is important to our overall understanding of the geology of large-impact basins on the lunar surface.

The Orientale basin has ~930 km in diameter and covers an area of ~700,0000 km^2 (Head 1974); within the basin, the largest Mare Orientale covers an area of ~52,700 km^2, and its volume is ~46,000 km^3 (Whitten et al. 2011). Previous studies estimated that the thickness of the Mare Orientale was less than ~1–2 km (Head 1974; Solomon and Head 1980) and possibly up to ~1 km (Greeley 1976; Scott et al. 1977). With the advent of recent LRO wide-angle Camera (LROC) image, the Digital Terrain Model of the Orientale basin and its spatial profiles have been established; the depth of the Maunder crater situated in the Mare Orientale is estimated as 6.04 km. Medium-Ti basalt flood eruptions fill much of the center of the Orientale basin (3.70 Ga) (Kadel et al. 1993). The location of the Mare Orientale (A), Lacus Veris (B), and Lacus Autumni (C) are shown in Fig. 2.1, and the sites selected for the analysis are marked in the square line.

The Lacus Veris has 396 km diameter and consists of five mare ponds, the largest of which covers an area of ~8,890 km^2 and the smallest of which is ~145 km. Lacus Veris (also called as Spring Lake) flat extent of North South lengthened shape. The crescent-shaped Lacus Veris is situated between the two mountainous rings constituting Montes Rook to the North and the floor filled with very dark material. Medium-Ti (<4 wt% TiO_2) basalt signatures are present in the northern

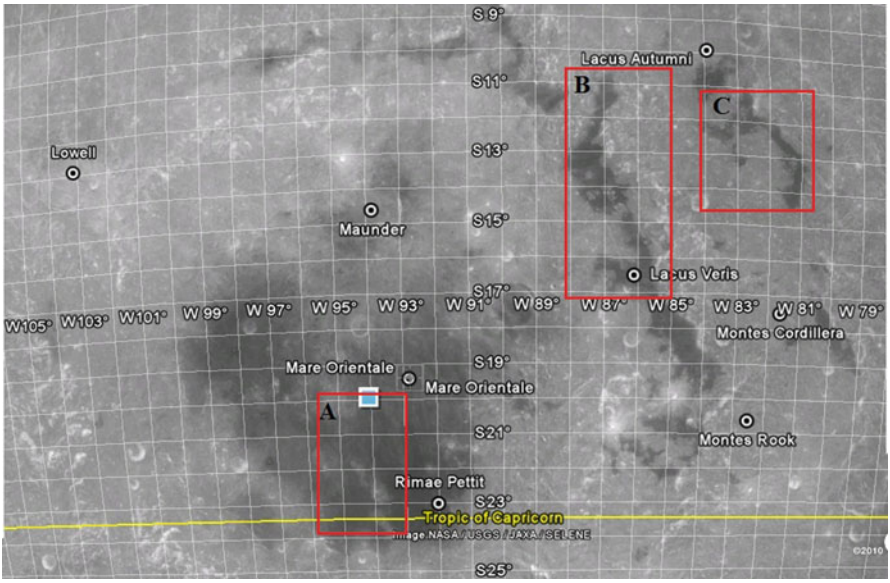

Fig. 2.1 Mare Orientale basin and test sites selected for the present study. The test sites are marked as (**A**) Mare Orientale South Central par, (**B**) Lacus Veris and (**C**) Lacus Autumni

and northeastern mare deposits of Lacus Veris, but medium–high (3–7 wt% TiO_2) basaltic signatures observed in the central and southern deposits (Kadel et al. 1993).

The Lacus Autumni is located between Montes Cordillera and Montes Rook and composed of several mare ponds. The largest of its three ponds covers an area of ~2,060 km^2 and the smallest is ~815 km^2 (Whitten et al. 2011). Medium–high (3–7 wt% TiO_2) basalt signatures observed for the northern mare deposits of Lacus Autumni, and medium-Ti (<4 wt% TiO_2) basalt signatures are present in the central and southern Lacus Autumni mare deposits (Kadel et al. 1993).

2.2.1 Objectives of the Study

The Mare Orientale, Lacus Veris, and Lacus Autumni of the Orientale basin basaltic regions were selected, and the following objectives were taken for the present study:

- TiO_2 estimation using Lucey's 1998 method.
- To quantify the lunar surface minerals such as clinopyroxene, orthopyroxene plagioclase and olivine using Moon Mineralogical Mapper Hyperspectral data and RELAB spectra.
- Establish the low-, medium-, and high -Ti basalt concentration map.
- Comparison of observed and RELAB basaltic spectra.
- Study of relation between TiO_2 content and age of the mare basalts.

When humans intend to establish lunar base, they will undoubtedly use the local rocks, minerals, and soils for construction materials and various chemical and metallurgical commodities (Chambers et al. 1995). The mineralogy of Orientale basin mare basalts is of particular interest, especially the question of how they compare with that on the nearside (Whitten et al. 2011). Morphological analysis result of Orientale basin basalts has been interpreted as emplacement of mare ponds during single eruptive events (Yingst and Head 1997). Several researchers have studied the Orientale basin basaltic composition, but none have been able to establish the actual mineralogy due to spatial and spectral limits of available data (Greeley et al. 1993; Kadel 1993; Staid 2000). Previous studies have found that Mare Orientale and associated mare ponds within the basin are highly contaminated with local highland material and concluded that Mare Orientale, Lacus Veris, and Lacus Autumni are probably of similar composition of lunar nearside basalts (Spudis et al. 1984; Staid 2000).

Yingst and Head (1997, 1999) found no obvious flow fronts and no distinct differences in mare composition in the individual ponds in Lacus Veris and Lacus Autumni, which assumed that individual mare ponds are the results of the single eruptive events. There is some indication of slight variation within the mare pond composition, which could either be due to lateral and vertical mixing of feldspathic material with mare soils or actual mineralogical differences (Kadel 1993; Staid 2000).

The wide range of TiO_2 contents within the returned samples has been used as a chemical property for separating them into groups including high- (>9 wt%, TiO_2), low- (1.5–9 wt% TiO_2), and very low-Ti (<1.5 wt% TiO_2) basalts, which generally cannot be related to the same source regions (Papike et al. 1998). The observed distribution of lunar basalt types suggests that mare volcanism was regionally complex with no simple correlation between composition and absolute age (e.g., Pieters 1978; Hiesinger et al. 2003, 2011).

Space weathering and mixing have altered the reflectance properties of the lunar surface over time; hence it is difficult to characterize the mineralogy of emplaced basalts from remote measurements of optically mature soils (Staid et al. 2011). In contrast, relatively crystalline and unweathered basaltic regolith associated with younger impact craters still retains diagnostic absorption features that can be interpreted based on measurements of returned lunar samples (Pieters 1977; McCord et al. 1981). M^3 data from Chandrayaan-1 have provided both the high spatial and spectral resolutions capable of investigating the detailed reflectance properties of small mare craters and allowed more direct characterization of basalt mineralogy than measurements of lunar soils that have been altered by space-weathering and non-mare contamination (Staid et al. 2011). Estimation of the relative abundance and composition of pyroxene and olivine will provide constraints on basaltic source regions, temporal evolution, and emplacement mechanisms.

2.3 Materials and Methods

India's first lunar mission Chandrayaan-1 Moon Mineralogical Mapper data, RELAB chemistry, and spectra were used in the present study. The Moon Mineralogy Mapper (M^3) is an imaging spectrometer developed by Brown University and the Jet Propulsion Laboratory, which sampled the lunar terrain from visible to near-infrared spectral region (400–3,000 nm), and provides high spatial and spectral resolution data for mineralogical study of the entire lunar surface (Goswami and Annadurai 2009). Remotely obtained reflectance spectra, combined with spectroscopic, chemical, and mineralogical data acquired in the Reflectance Experiment Laboratory (RELAB) from the lunar returned samples, can provide constraints on understanding and establishing compositional information about unexplored or unsampled planetary surfaces.

2.3.1 Methods

The methodology adopted in the study is shown in Fig. 2.2.

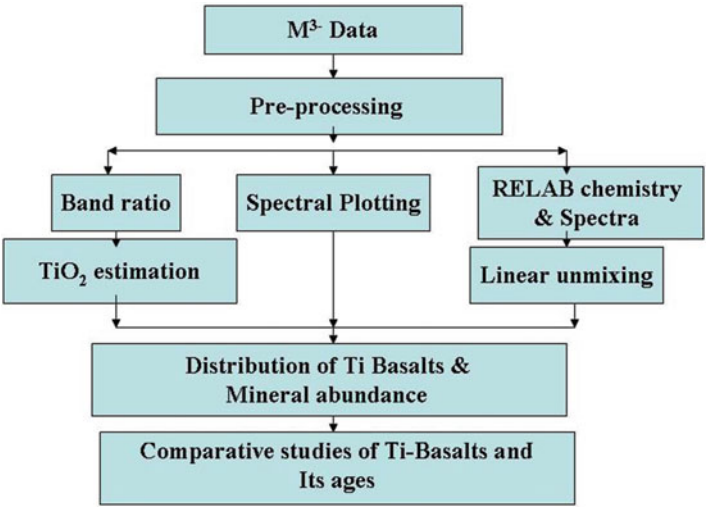

Fig. 2.2 The flow chart showing methodology adopted in the study

2.3.1.1 Data Acquisition and Preprocessing

The Orientale basin data has been downloaded from the orbital data explorer with reference to latitude and longitude information. The Chandrayaan-1 M^3 operates in two modes, including global mode and target mode. The data used here is acquired from global mode, which provides 85 bands in the spectral interval of 20–40 nm covering spectral range between 400 and 3,000 nm. The spatial resolution of global mode M^3 data is 140 m/pixel (Green et al. 2007; Pieters et al. 2009).

The preprocessing involves geo-referencing and apparent reflectance conversion from the given radiance. Using the glt file which carries information about latitude and longitude, the radiance data have been geo-referenced with ENVI software. Based on the method described by Staid et al. (2011), apparent reflectance was converted and bands were truncated at 2,500 nm, which also reduced additive contributions due to emissivity.

2.3.1.2 Spectral Profile

The mineralogy composition of the planetary surfaces has been investigated for decades using the visible and near-infrared (VISNIR) spectroscopy, owing to the abundance of diagnostic mineral absorptions in the electromagnetic spectrum (McCord et al. 1981; Pieters et al. 1996; Isaacson et al. 2011).Spectral reflectance

measurements are increasingly being used to investigate the surfaces of planetary bodies throughout the solar system. The reflectance spectra of rocks exhibit characteristic signatures depending upon the mineralogy, chemical composition, and physical properties. Remotely obtained spectra in the visible and near-infrared wavelength regions can provide information on the mineralogy and modal abundance of a planetary surface (Adams 1974, 1975). The minerals can be identified based on spectral features, including absorptions pattern, the parameter structures, absorption band positions, band strength, and band depth, which are directly related to mineral chemistry (Hunt and Salisbury 1970, 1971). The same principle can be adopted to map the mineralogical compositions of objects in the outer space. The visible and near-infrared reflectance spectra of mature lunar soils have been used to classify the mare basalts from the nearside of the moon (McCord et al. 1976; Pieters 1978; BVSP 1981).

The spectral profiles of the Mare Orientale, Lacus Veris, and Autumni were collected randomly from the preprocessed M^3 data. From the collected spectral profiles, the average spectrum has been taken for further analysis. From the spectra, it is observed that, there are two broad major absorption features at 950 and 2,100 nm due to dominance of clinopyroxene and minor amount of olivine content. Another insignificant absorption is located at 1,260 nm due to plagioclase content of the basaltic terrain. The spectra of the three test sites are shown in Fig. 2.3. To avoid the maturity effect of the mare soil in the spectra, the spectral profiles were collected in the fresh shallow impact craters. There is much variation observed in between the spectra from fresh shallow impact craters and that from the dark color matured mare soils. From the matured mare soil spectra, it is difficult to delineate the basaltic mineralogy.

Based on the morphological features, the spectral profiles have drawn for the preliminary understating of the rock types and their mineralogy. From this spectral profile, it has been understood that the dominant minerals of this region are

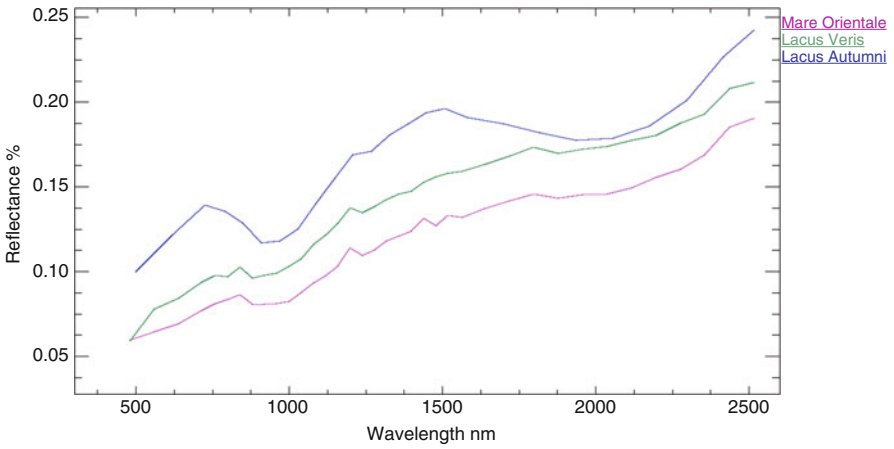

Fig. 2.3 Mare Orientale, Lacus Veris and Lacus Autumni spectra

plagioclase and clinopyroxene and the dominant rock types in this region are gabbroic anorthosite and anorthosite gabbro. These results have been validated through spectral mixing and unmixing through the available Apollo sample data.

2.3.1.3 TiO_2 Estimation

High-Ti mare soils are attractive resources for lunar liquid oxygen (LLOX) production because of their unconsolidated nature, high ilmenite abundance, and widespread occurrence (Chambers et al. 1995). There is much debate over whether to use mare soils or basalts as raw materials for mineral extraction, especially ilmenite (Heiken and Vaniman 1990; Taylor and McKay 1992). Ilmenite abundance in mare basalts and soils are an important resource in the lunar exploration projects. Chemically, mare basalts can be divided into two broad groups: (1) the older high-Ti group (age 3,550–3,850 Ma, TiO_2 content 9–13 %) and (2) the younger, low-Ti group (age 3,150–3,450 Ma, TiO_2 content 1–5 %). Experimental studies show that, the low-Ti basalts could have been derived from an olivine-pyroxene source rock at depths ranging from 200 to 500 km, while the high-Ti basalts could have been derived from olivine-pyroxene-ilmenite cumulates in the outer 150 km of the Moon (Papike et al. 1976).

The following algorithm derived by Lucey et al (1998) for estimation of TiO_2 weight percentage is used:

$$\theta_{\mathrm{Ti}} = \arctan\left(\frac{(R_{415}/R_{750}) - 0.45}{R_{750} - 0.05}\right) \tag{2.1}$$

$$\mathrm{TiO_2} = \left(\theta_{\mathrm{Ti}}^2 \times 20.79\right) - (\theta_{\mathrm{Ti}} \times 22.928) + 5.909 \tag{2.2}$$

Based on this analysis, it is observed that the percentage of TiO_2 weight in most of the Orientale basin basalts never varies more than 15 %.

Medium-Ti basalt flood eruptions have filled much of the center of the Orientale Basin (>3.70 Ga) and much of the Orientale is again flooded (<3.45 Ga) with medium–high-Ti basalts. The older medium-Ti basalts are exposed only in west-central Mare Orientale. The last eruptions in southern-east region of Mare Orientale are of high-Ti basalts (Kadel et al. 1993). Mare Orientale basalts bear high-Ti concentration and it's calculated through Lucey's 1998 algorithm and M^3 data. The south central portion's eastern region has TiO_2 in the range of 5–10 wt%, and the central region basalts have 10–12 wt % of TiO_2. In few places, the TiO_2 concentration exceeds up to 15 wt%. That most of the places in the Mare Orientale have >10 wt% of the TiO_2 indicates this region bearing high-Ti basalts. The spectral profile of the Mare Orientale basalts matching with RELAB's high-Ti mare soils spectra has confirmed the high-Ti basalts. The TiO_2 concentration map of the Mare Orientale is shown in Fig. 2.4a.

Hawke et al. (1991) calculated that Lacus Autumni and Lacus Veris' southern part bears lower-TiO_2 concentration, while the northern part of the Lacus Veris bears

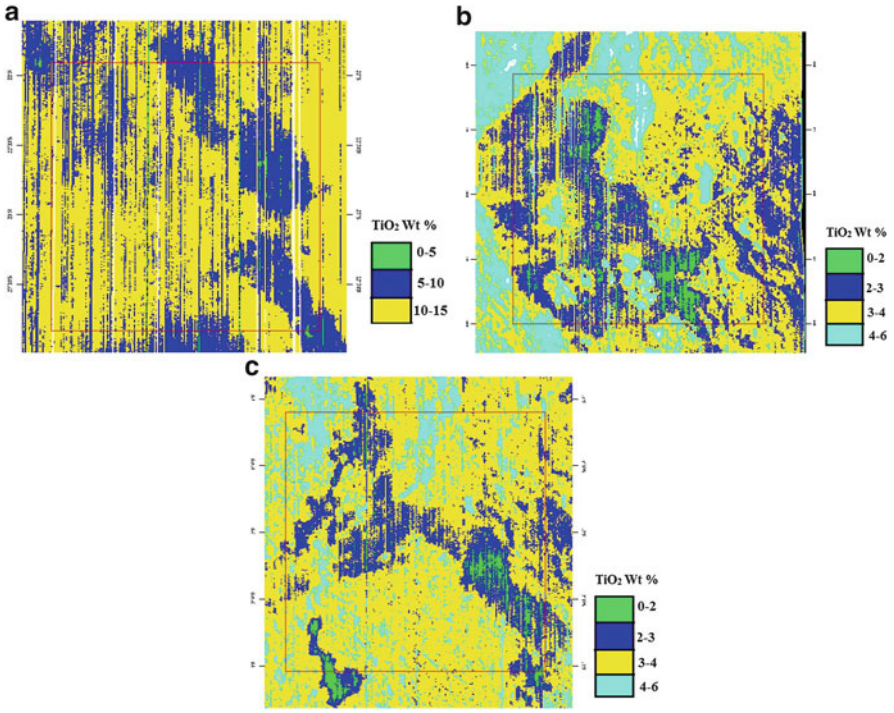

Fig. 2.4 TiO_2 wt % of (**a**). Mare Orientale, (**b**) Lacus Veris and (**c**) Lacus Autumni

intermediate-TiO_2 concentration. TiO_2 analysis of the center portion of the Lacus Veris indicates that, the region is dominated by the medium-Ti basalts in the range of <6 wt%. This is shown in Fig. 2.4b.

The Lacus Autumni also bears the medium-Ti basalts which concentration range is <6 wt%. The TiO_2 wt% of the Lacus Autumni is shown in Fig. 2.4c. The dominant basaltic region bears TiO_2 concentration range between 2–3 wt%. The variation of the Ti content observed in the spectral profile of the Lacus Autumni doesn't exceed 6 %.

2.3.1.4 Spectral Mixing and End-Member Selection

Manned and unmanned missions to the Moon have returned about 382 kg of lunar rocks and soils (Vaniman et al. 1991). These were collected from the lunar nearside's typical region, within and around the Procellarum KREEP Terrane (PKT) (Jolliff et al. 2000), or from equatorial latitudes on the eastern limb. Linear spectral mixture analysis can be used to model the spectral variability in multispectral or hyperspectral images and to establish the relation of its results and the physical abundance of surface constituents represented by the spectral

end-members (Tompkins et al. 1997). In order to use a linear mixture model, the spectral reflectance of the "pure" end-members should be measured. Ideally, ground-based reflectance spectra would be acquired from the known minerals and rocks to produce accurate end-members. Since we are concentrating the lunar surface, we are not able to provide the specific high-precision ground truth information/spectra at this present situation. Spectral mixture analysis (SMA), a technique based on modeling image spectra as the linear combination of end-members, has been used to derive the fractional contribution of end-member materials to image spectra in a wide variety of applications. An end-member is a "pure" spectrum of a material or target and has a unique spectral signature. Image end-members are pure pixels from image itself. The end-member selection included the following components: plagioclase, ortho-/clinopyroxene, and olivine in the mineral class and low-, medium-, and high-Ti basalts in rock classes. Performing spectral unmixing requires appropriate end-member selection, since unsuitable end-member may lead to meaningless fraction mapping. In this paper, seven end-members have been identified and extracted from the image data for spectral unmixing analysis.

The bidirectional reflectance spectra of low-, medium-, and high-Ti basaltic soils acquired from various grain sizes such as <10, 10–20, 20–45, and <45 μm. Based on the grain size variation, there is not much variation observed in the spectral curves apart from the broad weak absorption near 1,000 nm for the grain size of 20–45 μm sample. To establish the basaltic end-member's spectra, the RELAB spectra of low-, medium-, and high-Ti basalts of various grain sizes have been taken and averaged. The spectral values are averaged for the various grain sizes, and one spectral end-member is derived for each basaltic soil. The average of the bulk chemical composition in oxides and in modal abundance of minerals in the various grain sizes of low Ti (15071-52), medium Ti (12030-14), and high Ti (71501-35) is given in Tables 2.1 and 2.2, respectively. The spectral profiles of RELAB mineral end-member (a) and basaltic end-members (b) are shown in Fig. 2.5. The spectra from 450 to 2,500 nm are used as end-member to estimate the abundance of the various basalts in the Orientale basin basaltic terrain. Apart from the basalts, the plagioclase, ortho-/clinopyroxene, and olivine spectra from RELAB are also utilized in the present study.

2.3.1.5 Linear Spectral Unmixing

Spectral unmixing methods have been proven useful in the application of imaging spectroscopy for geological studies. It is understand that, grain size effects intimate mixtures and mineral coatings, so other spectroscopic spectral unmixing methods have proven useful in the application of imaging spectroscopy to geological studies. Linear spectral unmixing (LSU) has been proposed for the analysis of hyperspectral images to compute the fractional contribution of the detected end-members to each pixel in the image. Linear spectral unmixing is used to discriminate one type of material from another. It provides an estimation of how much material available in a pixel and a method of classifying broad categories of materials in a pixel.

Table 2.1 The average bulk chemistry of low, medium, and high-Ti basalts of various grain sizes such as <45, 20–45, 10–20, and <10 μm

Bulk chemistry (oxides wt %)	Low-Ti basalt (15071)-52	Medium-Ti basalt (12030)-14	High-Ti basalt (71501)-35
SiO_2	46.07	46.25	31.87
TiO_2	1.89	3.32	9.52
$Al2O_3$	13.87	11.70	11.83
$Cr2O_3$	0.44	0.43	0.43
MgO	10.88	9.42	9.49
CaO	10.52	9.78	10.36
MnO	0.19	0.20	0.22
FeO	13.87	16.27	16.05
Na_2O	0.40	0.46	0.38
K_2O	0.16	0.29	0.09
P_2O_5	0.15	0.25	0.06
SO_2	0.11	0.12	0.19

Source: RELAB

Table 2.2 The average modal abundance of minerals for low-, medium-, and high-Ti basalts of various grain sizes such as <45, 20–45, 10–20, and <10 μm

Modal abundance of minerals (wt %)	Low-Ti basalt (15071)-52	Medium-Ti basalt (12030)-14	High-Ti basalt (71501)-35
Ilmenite	1.63	2.93	9.86
Plagioclase	19.10	15.76	18.76
Pyroxene	16.56	23.50	14.60
Olivine	2.86	3.50	3.40
Agglutinitic glass	52.16	48.06	45.40
Volcanic glass	3.90	1.43	6.70
Others	3.76	4.80	1.30

Source: RELAB

A specific problem of LSU is the determination of the end-members; to this end we employ two approaches: the Convex Cone Analysis and another one based on the detection of morphological independence. The planetary surface materials have specific spectral features, which are related to their composition. Each image pixel is assumed to be some mixture of various component materials, but regular algorithms for classification cannot identify more than one class within one pixel. Hence, the spectral unmixing is used to deal with this case.

Quantitatively retrieving mineral abundances from hyperspectral data is one of the promising and challenging geological application fields of hyperspectral remote sensing. However, its mixture characteristic of mineral spectra and deconvolution method of mixture spectra are the most basic obstacles in using hyperspectral data

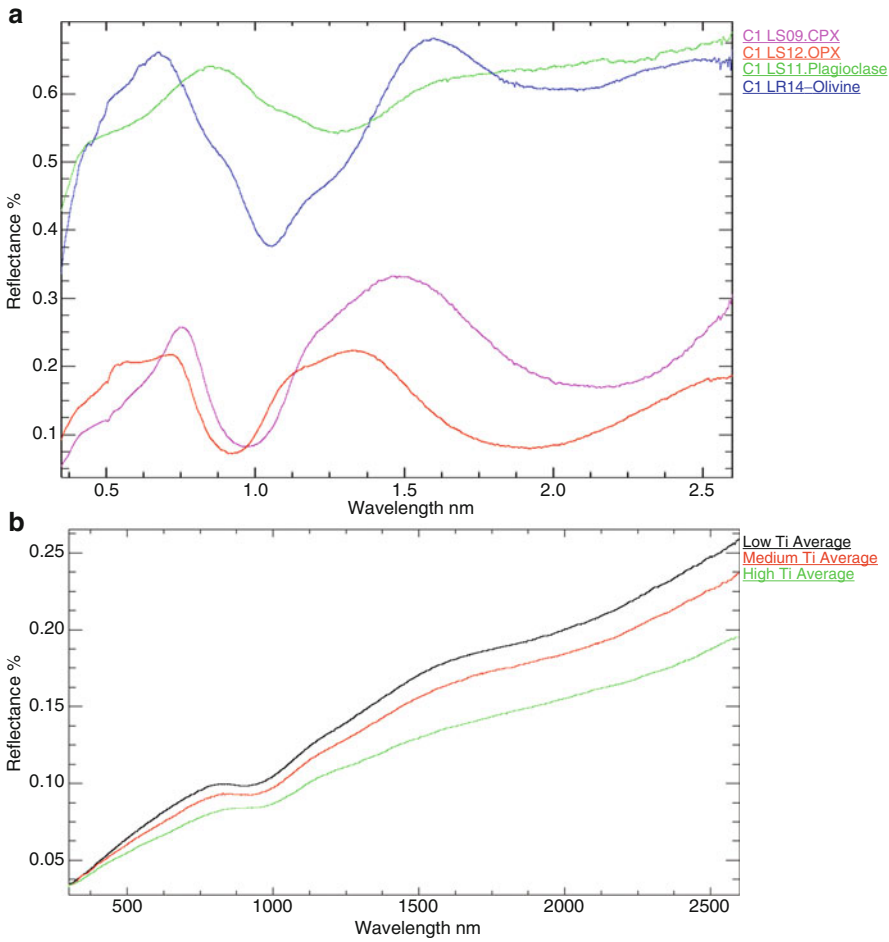

Fig. 2.5 (**a**) RELAB spectra of plagioclase, clino/ortho pyroxene and olivine minerals. (**b**) Low-, medium- and high-Ti basaltic end member spectra from RELAB

(Bokun et al. 2008). Pure materials can be measured under controlled conditions in the laboratory, but for remotely sensed data, multiple components possibly will be included in one measurement (pixel) causing spectral mixing.

2.4 Results and Discussion

Based on the spectral profiles, we are able to discriminate the difference between the ortho- and clinopyroxene such as Mg, Fe, and Ca pyroxenes. Based on the TiO_2 estimation, spectral profiles, and linear spectral unmixing, the following results were obtained and discussed herewith.

2.4.1 *Mare Orientale*

The averaged low-, medium-, and high-Ti basaltic spectra have been derived from the RELAB mare soil spectra. The bulk chemistry and modal abundance of the minerals have been listed in Table 2.1 and 2.2, respectively. Based on the RELAB basaltic spectra, the concentration of the different types of basalts is mapped in the Mare Orientale, Lacus Autumni, and Lacus Veris basaltic regions. The south central part of the Mare Orientale is comprised of high-Ti basalts ranges around 21 % and medium-Ti basalts dominant in 40 %, and in few craters it leads upto 60 % and low-Ti basalts ranges around 6 %. The comparative analysis of the different types of basalts is given in Table 2.3. The concentration of the high-Ti basalts and medium-Ti basalts is shown in Fig. 2.6a, b.

Compared with the Lacus Autumni and Veris, the south central part of the Orientale basalts bears high-Ti basalts, which ranges up to 15 %. Hence, based on the TiO_2 concentration, the Lacus Autumni and Veris might be of the same origin and similar ages.

In the south central part of the Mare Orientale basaltic region, the soil consists of <20 % of plagioclase. Some impact craters located in the inner side of the

Table 2.3 The observed Modal abundance of minerals for Mare Orientale, Lacus Autumni and Lacus Veries from M^3 data

Modal abundance of minerals and Ti-basalts (values are in wt %)	Mare Orientale	Lacus Autumni	Lacus Veris
Plagioclase	20	21	12
Pyroxene (CPX +OPX)	21	32	21
Olivine	4	4	2.5
Ilmenite	–	–	–
Agglutinitic glass	–	–	–
Volcanic glass	–	–	–
Others	–	–	–
Basalts			
High-Ti basalts	21	10	40
Medium-Ti-basalts	60	–	–
Low-Ti basalts	6	21	>60
Modal abundance of minerals (wt %)	Mare Orientale	Lacus Autumni	Lacus Veries
Ilmenite	–	–	–
Plagioclase	20	21	12
Pyroxene	21	32	21
Olivine	4	4	2.5
Agglutinitic glass	–	–	–
Volcanic glass	–	–	–
Others	–	–	–

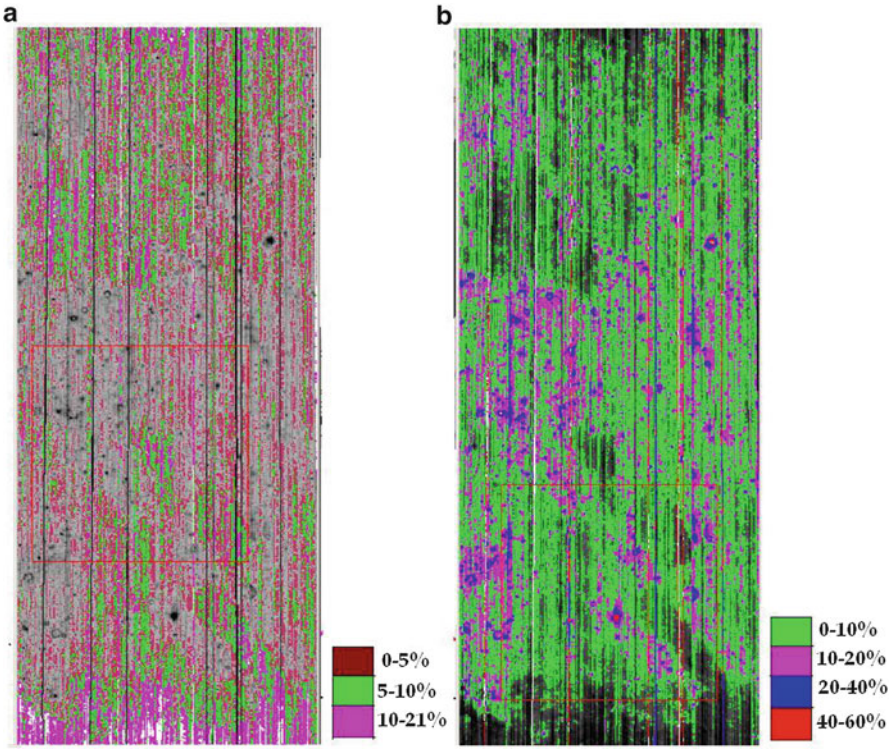

Fig. 2.6 High Ti (**a**) and medium Ti (**b**) basalts distribution map of South Central region of Mare Orientale

basaltic regions contain plagioclase in the range of up to 40 %, which excavated the highland material from deeper crust. In the central part of the Mare Orientale region, clinopyroxene is the dominant mineral which ranges from 8–12 % to 22 %, and this almost consistent with pyroxene content of the high-Ti basalts of RELAB samples. There is no measurable amount of orthopyroxene observed in the south central part of the Mare Orientale. Olivine content of the south central part of Mare Orientale varies from 2 to 4 %.

2.4.2 Lacus Veris

The high-Ti-bearing basalt concentration range is up to 40 % in the Lacus Veris region. The region is dominated by high-Ti basalts which accounts for 27 %. Like Lacus Autumni, this region also does not have much medium-Ti basaltic concentration. The entire western region of the Lacus Veris is dominated by low-Ti-bearing basalts. The distribution of the high- and low-Ti basalts is shown in Fig. 2.7a, b, respectively.

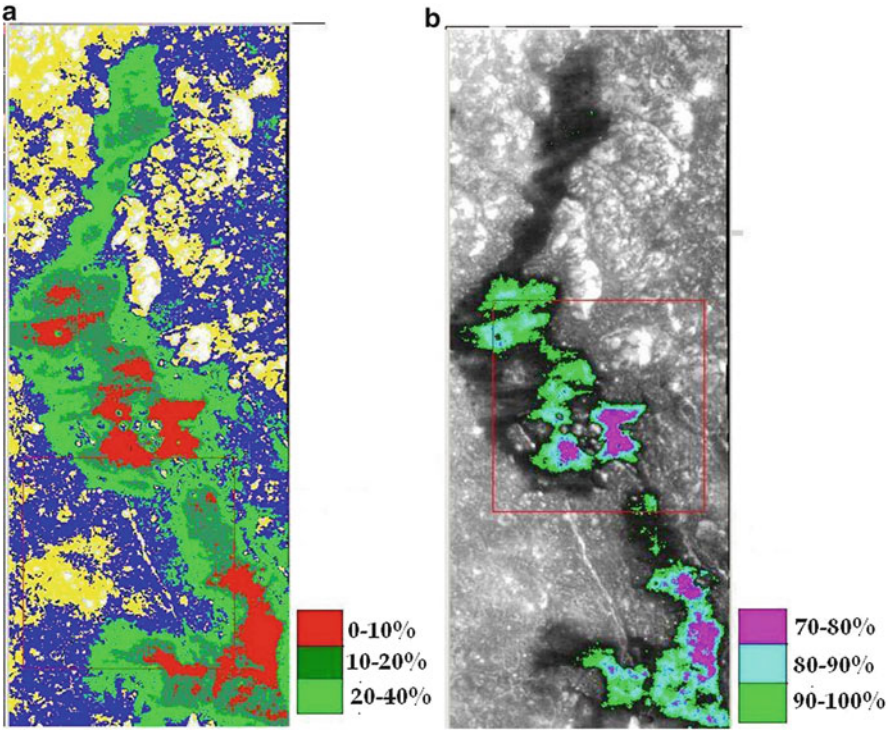

Fig. 2.7 High-Ti (**a**) and low-Ti (**b**) basalts distribution map of Lacus Veris

The concentration of the CPX is 15 % in the Lacus Veris basaltic terrain. In some places, it exceeds up to 21 %. This is almost similar with the high-Ti basaltic chemistry of the RELAB sample no. 71501-35 in the grain size of 20–45 μm. Like previous test sites, the Lacus Veris also does not have much amount of OPX. The plagioclase content of this region is comparatively lesser than the Mare Orientale and Lacus Autumni. The plagioclase and olivine content in the Lacus Veries basaltic region is around 12 % and 2.5 % respectively. The olivine distribution is observed only in the small areas of the Lacus Veries basaltic region. The concentration of the olivine is in and around 2.5 % in the Lacus Veris region. That is also presented in small areas and not distributed in the all basaltic region.

2.4.3 Lacus Autumni

The high-Ti basaltic concentration of Lacus Autumni region is shown in Fig. 2.8a. The Lacus Autumni consists of only 10 % of the high-Ti basalts, however in some specific regions, the content of the high-Ti basalts is increased up to 80 %, which is marked in magenta color shown in the Fig. 2.8a. Low-Ti basalts concentrated in

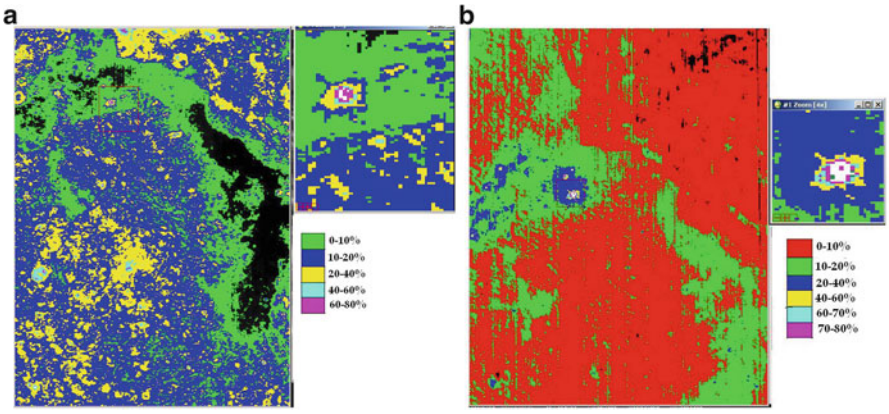

Fig. 2.8 High-Ti (**a**) and low-Ti (**b**) basalts distribution map of Lacus Autumni

the range of 21 % in most of the Lacus Autumni, but in some specific locations, the content of the Low-Ti basalts exceeds up to 70–80 %, which is shown in Fig. 2.8b in the colors of cyan and magenta. There is no much amount of medium-Ti basalt distribution in the Lacus Autumni region.

The clinopyroxene (CPX) in the central part of the Lacus Autumni is around 32 %. The outside of the Lacus Autumni, CPX concentration varies in the range from 32 to 42 %. The southern-east portion of the Lacus Autumni has slightly lower CPX with the amount of 26 %. There is no much amount of OPX measured in the Lacus Autumni region. The plagioclase content of the Lacus Autumni is 27 %, 21 % in central part and 30 % in external side of the Lacus Autumni. The olivine concentration of the Lacus Autumni is nearly 4 %. The western portion of the Lacus Autumni has lower olivine content compared to the central portion. The impact craters on the Lacus Autumni have slightly higher olivine content that is nearly up to 5 %. It could be due to excavation of deeper material due to impact.

2.4.4 Age of Mare Orientale, Lacus Veris, and Lacus Autumni

Compared with lunar highland, mare basalts occupy lesser area, but they contain much information about the thermal history of the moon and the nature of the lunar interior (Head 1976). The age of mare basalts studied is between 3.15 and 3.96 Gy. But recent photogeologic (crater-counting) studies indicate that there are 2.5-Gy-old younger basalts on the moon, which yet to be sampled. The returned samples were classified into two broad categories based on the TiO_2 concentration: high-titanium group (ages ~3.55–3.85 Gy; TiO_2, 9–14 wt%) and the low-titanium group (ages 3.15–3.45 Gy; TiO_2, 1–5 wt%). Basalts returned by Apollo 11 and 17 are dominated by high-titanium group including olivine and ilmenite, whereas Apollo 12 and 15 and Luna 16 returned samples dominated by low-titanium group which is almost olivine (Head 1976).

M^3 images with high spatial and spectral resolution can be used to count the craters for given size on the Mare Orientale, Lacus Veris, and Lacus Autumni and to produce the reliable model. In mare Orientale, craters >5 km were counted on the Hevelius formation and craters >0.75 km were counted on the Maunder formation. This crater count method calculated that ages are ~3.68 Ga for the ejecta and ~3.64 Ga for the melt sheet. Orientale was emplaced shortly after the Maunder formation in ~3.58 Ga. This delay of ~60–100 Ma between basin formation and volcanism in three study areas argues against Orientale impact-pressure-release melting ages (Whitten et al. 2011).

In the Lacus Veris, the crater count chronology deduced the age of five largest ponds in the range of ~3.20 to ~3.69 Ga (Whitten et al. 2011), which is consistent with the previous studies conducted by Greeley et al. (1993) and Kadel (1993).

In the Lacus Autumni, crater counts give an age range between ~3.47 and ~1.66 Ga (Whitten et al. 2011). The young model age of ~1.66 Ga falls well within the calculated time range of mare volcanism occurring on the lunar nearside (Hiesinger et al. 2000). This discrepancy in the model ages could be the result of sizeable differences in the definition of the count area or count statistics used. The detailed discussion can be found in Whitten et al. (2011) and relevant references.

2.4.5 Validation

The results revealed from the RELAB spectra and chemical data have been used to validate the result of this present research. Apart from the RELAB data, the results have been compared with the previous Clementine UVVIS data global mineral mapping study conducted by Bokun et al 2010. The RELAB low-, medium-, and high-Ti basaltic spectra were compared with Mare Orientale, Lacus Veris, and Autumni spectra established from M^3 data, which is shown in Fig. 2.9. In this,

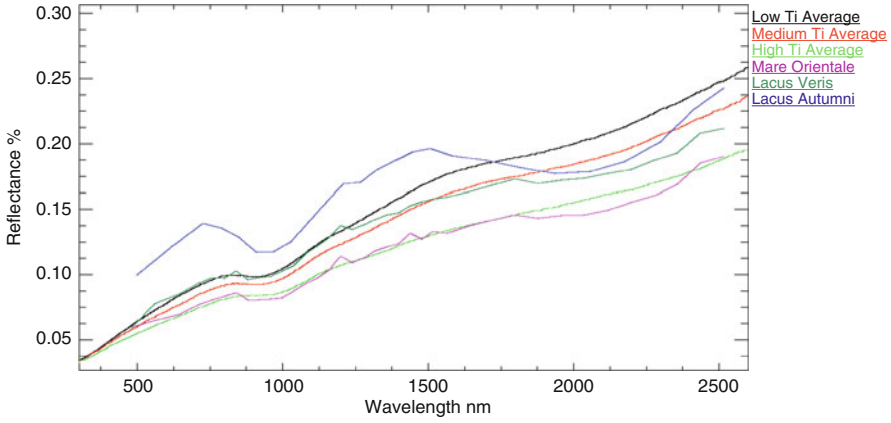

Fig. 2.9 Low-, medium- and high-Ti basalts spectra with Mare Orientale, Lacus Veris and Lacus Autumni spectra

the Mare Orientale spectra almost match with the RELAB high-Ti basaltic spectra. The Lacus Veris spectrum is plotted in between the low- and medium-Ti RELAB basaltic spectra. The Lacus Autumni spectra were not matched with this group of basaltic spectra, and it indicates admixing and contamination of the maria regolith with materials excavated or ejected from underlying and neighboring rocks in the Lacus Autumni region.

2.5 Conclusion and Future Work

Since the RELAB basaltic samples were brought from the nearside of the moon, there may be slight variation in the Orientale basin basalts. Apollo geochemical ground tracks and sample collection did not cover this region; hence, the relative end-member spectral library and chemistry such as plagioclase, ortho- and clinopyroxenes, and olivine and low-, medium-, and high-Ti basalts are only used. The more precise results can be provided once we get samples from Orientale basalts.

The spectral mixtures were derived from RELAB spectra, based on lunar rock classification, and they are considered as end-members for estimating the abundance of the rock content in the specified area using M^3 data. If there are similar kinds of studies for the other basaltic terrain on the lunar surface, the results can be used as validation. However, only the global lunar mineral mapping maps using the UVVIS multispectral Clementine data are available at present, so the current results have been validated with RELAB chemistry.

To improve this work, it is important to compare the fraction covers with field data in order to verify the data obtained through the images. In addition, field spectral data is necessary for end-member selection, because a good choice of end-members is the most important step for a good spectral unmixing. Mixed pixels may cover a region containing different components, and therefore, traditional image classification approach should be altered, which assigns a particular class of ground cover to each pixel (Kanniah et al. 2001).

Low-Ti basalts are younger than the high-Ti basalts. But remote sensing data based studies suggests that high-Ti basalts are younger. Finally, there is no obvious correlation between the ages and low-Ti and high-Ti concentrations (e.g., Pieters 1978; Hiesinger et al. 2003, 2011). Based on the TiO_2 analysis, the Mare Orientale basalts have high-TiO_2 ($\sim$15 %) content compared with the Lacus Veris and Lacus Autumni (<6 %). Papike et al. (1976) has concluded that the Mare Orientale age is older than the Lacus Veris and Lacus Autumni, which supports the result of crater counting given by Whitten et al. (2011). In the future, if we obtain sample from the Orientale basin, with radiometric dating and geochemical measurements, we will get precise chronology of the Orientale basin and clarify the relation between the TiO_2 content and ages. In mineral mapping, all basaltic terrains from the Orientale basin are dominant with clinopyroxene followed by plagioclase.

The future work will focus on the thermal and photometrically corrected data, which would be used to estimate the minerals and mineral mixtures using Hapke's single-scattering albedo (SSA) modeling and spectral unmixing. The error of

mineral abundances derived from reflectance spectra and single-scattering albedo is 20.05 % and 5.03 %, respectively (Bokun et al. 2008). Since the significant variation between the linear spectral unmixing and single-scattering albedo, SSA should be employed for getting more accuracy in quantitative mapping. Once corrections are done, the Modified Gaussian Model (MGM) could perform to derive the modal percentage of the subset of Mg-Fe and Ca pyroxenes and olivine, which will obtain the better results.

Acknowledgement The author acknowledges PLANEX, Physical Research Laboratory (ISRO), Ahmedabad, and Council of Scientific and Industrial Research (CSIR), New Delhi, for Postdoctoral Research Fellowship. Moreover, the author thanks the anonymous reviewer's critical review which helps to improve the paper.

References

Abdul S (2003) Subpixel classification of ground surface features. GIS Dev 7(11):20–24

Adams JB (1974) Visible and near-infrared diffuse reflectance spectra of pyroxenes as applied to remote sensing of solid objects in the solar system. J Geophys Res 79:4829–4836

Adams JB (1975) Interpretation of visible and near-infrared diffuse reflectance spectra of pyroxenes and other rock-forming minerals. In: Karr C Jr (ed) Infrared spectroscopy of lunar and terrestrial minerals. Academic, New York, pp 91–116

Basaltic Volcanism Study Project (BVSP) (1981) Basaltic volcanism on the terrestrial planets. Pergamon Press, Oxford, p 1286 (Heiken GH, Vaniman DT, French BM (eds) (1991) Lunar sourcebook. Cambridge University Press, Cambridge, p 736)

Boardman JW (1989) Spectral and spatial unmixing: applications of singular value decomposition. In: Proceedings of image processing, Reno, 1989

Bokun Y, Shengweia L, Runsheng W, Xiaofanga G, Weidongb S (2008) Experiment study on quantitative retrieval of mineral abundances from reflectance spectra, remote sensing of the environment: 16th national symposium on remote sensing of China (eds) Qingxi Tong Proceedings of SPIE, vol 7123, p 712303. doi:10.1117/12.815549

Bokun Y, Runsheng W, Fuping G, Zhenchao W (2010) Minerals mapping of the lunar surface with Clementine UVVIS/NIR data based on spectra unmixing method and Hapke model. ICARUS 208:11–19

Chambers JG, Taylor LA, Patchen A (1995) Quantitative mineralogical characterization of lunar high-TI mare basalts and soils for oxygen production. J Geophys Res 100(E7):14391–14401

Chen X, Warner T, Campagna D (2007) Integrating visible, near-infrared and short-wave infrared hyperspectral and multispectral thermal imagery for geological mapping at Cuprite, Nevada [J]. Remote Sens Environ 110:344–356

Clark R, Swayze G, Livo R, et al (2003) Imaging spectroscopy: Earth and planetary remote sensing with the USGS Tetracorder and expert systems [J]. J Geophys Res 108(E2):5–1 to 5–44

Clark RN et al (2008) Compositional mapping of Saturn's satellite Dione with Cassini VIMS and implications of dark material in the Saturn system. Icarus 193:372–386

Cloutis EA, Gaffey MJ (1991) Pyroxene spectroscopy revisited: spectral compositional correlations and relationships to geothermometry. J Geophys Res 96:22809–22826

Crown DA, Pieters CM (1987) Spectral properties of plagioclase and pyroxene mixtures and the interpretation of lunar soil spectra. ICARUS 72:492–506

Goswami JN, Annadurai M (2009) Chandrayaan-1: India's first planetary science mission to the Moon. Curr Sci 96(4):486–491

Greeley R (1976) Modes of emplacement of basalt terrains and an analysis of mare volcanism in the Orientale Basin. In: Proceedings of the 7th lunar science conference, Houston, TX, 15–19 March 1976, vol 3 (A77-34651 15-91). Pergamon Press, Inc., New York, pp 2747–2759

Greeley R et al (1993) Galileo imaging observations of lunar maria and related deposits. J Geophys Res 98:17183–17205. doi:10.1029/93JE01000

Green RO, Pieters CM, Mouroulis P, Sellars G, Eastwood M, Geier S, Shea J (2007) The Moon Mineralogy Mapper: characteristics and early laboratory calibration results. Lunar Planet Sci [CD-ROM] 38, Abstract 2354

Hawke BR, Lucey PG, Taylor GJ, Bell JF, Peterson CA, Blewett DT, Horton K, Smith GA, Spudis PD (1991) Remote sensing studies of the Orientale region of the Moon: a pre-Galileo view. Geophys Res Lett 18(11):2141–2144

Head JW (1974) Orientale multi-ringed basin interior and implications for the petrogenesis of lunar highland samples. Moon 11:327–356. doi:10.1007/BF00589168

Head JW (1976) Lunar volcanism in space and time. Rev Geophys 14(4):265–300. doi:10.1029/RG014i002p00265

Heiken GH, Vaniman DT (1990) Characterization of lunar ilmenite resources. In: Proceedings of the 20th lunar and planetary science conference, Houston, TX, 13–17 March 1989 (A90-33456 14-91). Lunar and Planetary Institute, Houston, pp 239–247

Hiesinger H, Jaumann R, Neukum G, Head J (2000) Ages of mare basalts on the lunar nearside. J Geophys Res 105(E12):29239–29275

Hiesinger H, Head JW, Wolf U, Jaumann R, Neukum G (2003) Ages of lunar mare basalts in Mare Frigoris and other nearside maria, Lunar Planet Sci [CD-ROM], 34, Abstract 1257

Hiesinger H, Head III JW, Wolf U, Jaumann R, Neukum G (2011) Ages and stratigraphy of lunar mare basalts: a synthesis. In: Ambrose WA, Williams DA (eds) Recent advances and current research issues in lunar stratigraphy, Special paper, vol 447. Geological Society of America, pp 1–51. doi:10.1130/2011.2477(01)

Hunt GR, Salisbury JW (1970) Visible and near infrared spectra of minerals and rocks. I. Silicate minerals. Mod Geol 1:283–300

Hunt GR, Salisbury JW (1971) Visible and near infrared spectra of minerals and rocks. II. Carbonates. Mod Geol 2:23–30

Isaacson PJ, Pieters CM, Besse S, Clark RN, Head JW, Klima RL, Mustard JF, Petro NE, Staid MI, Sunshine JM, Taylor LA, Thaisen KG, Tompkins S (2011) Remote compositional analysis of lunar olivine-rich lithologies with Moon Mineralogy Mapper (M^3) spectra. J Geophys Res 116:E00G1. doi:10.1029/2010JE003731

Jolliff BL, Gillis JJ, Haskin LA, Korotev RL, Wieczorek MA (2000) Major lunar crustal terranes: surface expressions and crust-mantle origins. J Geophys Res 105:4197–4216

Kadel SD (1993) Multispectral and morphologic analyses of lunar mare basalts in the Orientale Basin, M.Sc., Arizona State University, Phoenix

Kadel SD, Greeley R, Neukum G, Wagner R (1993) The history of mare volcanism in the Orientale Basin; mare deposit ages, compositions and morphologies, Lunar Planet Sci [CD ROM], 24, Abstract 1374

Kanniah KD, Ng Su Wai, Alvin Lau Meng Shin, Abd Wahid Rasib (2001) Linear mixture modelling applied to IKONOS data for mangrove mapping. http://www.a-a-r-s.org/acrs/proceeding/ACRS2005/Papers/FRR2-2.pdf

LeMouélic SL, Langevin Y (2001) The olivine at the lunar crater Copernicus as seen by Clementine NIR data. Planet Space Sci 49:65–70

LeMouélic SL, Langevin Y, Erard S (1999) The distribution of olivine in the crater Aristarchus inferred from Clementine NIR data. Geophys Res Lett 26:1195–1198

Lucey PG, Blewett DT, Hawke BR (1998) Mapping the FeO and TiO_2 content of the lunar surface with multispectral imagery. J Geophys Res 103(E2):3679–3699

Lucey PG et al (2006) Understanding the lunar surface and space – Moon interactions. Rev Miner Geochem 60:83–219. doi:10.2138/rmg.2006.60.2

McCord TB, Charette MP, Johnson TV, Lebofsky LA, Pieters C, Adams JB (1972) Lunar spectral types. J Geophys Res 77:1349–1359

McCord TB, Pieters CM, Feierberg MA (1976) Multispectral mapping of the lunar surface using ground based telescopes. Icarus 29:1–34

McCord TB, Clark RN, Hawke BR, Mcfadden LA, Owensby PD, Pieters CM, Adams JB (1981) Moon: near-infrared spectral reflectance, a first good look. J Geophys Res 86(B11):10883–10892

Papike JJ, Hodges FN, Bence AE, Cameron M, Rhodes JM (1976) Mare Basalts' crystal chemistry, mineralogy, and petrology. Rev Geophys 14(4):475–540

Papike JJ, Ryder G, Schearer CK (1998) Lunar samples. In: Papike JJ (ed) Planetary materials. Mineralogical Society of America, Washington, DC

Pieters CM (1977) Characterization of lunar mare basalt types-II: spectral classification of fresh mare craters. In: Proceedings of the 8th lunar science conference, Houston, TX, 14–18 March 1977, vol 1 (A78-41551 18-91). Pergamon Press, Inc., New York, pp 1037–1048

Pieters CM (1978) Mare basalt types on the front side of the Moon: a summary of spectral reflectance data. In: Proceedings of the ninth lunar and planetary science conference, pp 2825–2849

Pieters CM, Englert PA (eds) (1997) Remote geochemical analysis: Elemental and mineralogical composition. Cambridge University Press, New York, p 467

Pieters CM, Head JW, Sunshine JM, Fischer EM, Murchie SL, Belton M, McEven A, Gaddis L, Greeley R, Neukum G, Jaumann R, Hoffmann H (1993) Crustal diversity of the Moon: compositional analyses of Galileo solid state imaging data. J Geophys Res 98:17127–17148. doi:10.1029/93JE01221

Pieters CM, Mustard JF, Sunshine JM (1996) Quantitative mineral analyses of planetary surfaces using reflectance spectroscopy. Spec Publ Geochem Soc 5:307–325

Pieters CM, Head JW, Gaddis L, Duke M (2001) Rock types of South Pole-Aitken Basin and extent of basaltic volcanism. J Geophys Res 106(E11):28001–28022

Pieters CM, Klima RL, Hiroi T, Dyar MD, Lane MD, Treiman AH, Noble SK, Sunshine JM, Bishop JL (2008) Martian dunite NWA 2737: integrated spectroscopic analyses of brown olivine. J Geophys Res 113(1–12):E06004

Pieters CM, Boardman J, Buratti B, Chatterjee A, Clark R, Glavich T, Green R, Head J, Isaacson P, Malaret E, McCord T, Mustard J, Petro N, Runyon C, Staid M, Sunshine J, Taylor L, Tompkins S, Varanasi P, White M (2009) The Moon Mineralogy Mapper (M^3) on Chandrayaan-1, Indian Academy of Sciences. Curr Sci 96(4):500–505

Scott DH, McCauley JF, West MN (1977) Geologic map of the west side of the moon, Miscellaneous investigations series map I-1034. U.S. Geological Survey, Reston

Shkuratov Y, Opanasenko N, Zubko E, Grynko Y, Korokhin V, Pieters C, Videen G, Mall U, Opanasenko A (2007) Multispectral polarimetry as a tool to investigate texture and chemistry of lunar regolith particles. Icarus 187:406–416

Solomon SC, Head JW (1980) Lunar mascon basins: Lava filling, tectonics, and evolution of the lithosphere. Rev Geophys Space Phys 18:107–141. doi:10.1029/RG018i001p00107

Spudis PD, Hawke BR, Lucey P (1984) Composition of Orientale Basin deposits and implications for the lunar basin-forming process. In: Proceedings of the 15th lunar planetary science conference, Part 1, J Geophys Res 89(Suppl):C197–C210

Staid MI (2000) Remote determination of the mineralogy and optical alteration of lunar basalts using clementine multispectral images; global comparisons of mare volcanism. Ph.D. thesis, Brown University, Providence, RI

Staid MI, Pieters CM (2000) Integrated spectral analysis of mare soils and craters: applications to eastern nearside basalts. Icarus 145:122–139. doi:10.1006/icar.1999.6319

Staid MI, Pieters CM, Head JW (1996) Mare Tranquillitatis: Basalt emplacement history and relation to lunar samples. J Geophys Res 101:23213–23228. doi:10.1029/96JE02436

Staid MI et al (2011) The mineralogy of late stage lunar volcanism as observed by the Moon Mineralogy Mapper on Chandrayaan-1. J Geophys Res. doi:10.1029/2010JE003735

Taylor SR (1975) Lunar science: a post-Apollo view. Pergamon, New York, p 372

Taylor LA, McKay DS (1992) An ilmenite feedstock on the moon; beneficiation of rocks versus soils In: Proceedings of the 23rd lunar and planetary science conference, League City, TX, 16–20 March 1992, Lunar and Planetary Institute, Houston, TX, pp 1411–1412

Tompkins S, Mustard JF, Pieters CM, Forsyth DW (1997) Optimization of endmembers for spectral mixture analysis. Remote Sens Environ 59(3):472–489

Vaniman D, Dietrich J, Taylor GJ, Heiken G (1991) Exploration, samples, and recent concepts of the moon. In: Heiken GH, Vaniman DT, French BM (eds) Lunar sourcebook: a user's guide to the moon. Cambridge University Press/Lunar and Planetary Institute, New York

Whitten J, Head JW, Staid M, Pieters CM, Mustard J, Clark R, Nettles J, Klima RL, Taylor L (2011) Lunar mare deposits associated with the Orientale impact basin: new insights into mineralogy, history, mode of emplacement, and relation to Orientale Basin evolution from Moon Mineralogy Mapper (M^3) data from Chandrayaan-1. J Geophys Res 116:E00G09. doi:10.1029/2010JE003736

Yingst RA, Head JW (1997) Volumes of lunar lava ponds in South Pole–Aitken and Orientale basins: implications for eruption conditions, transport mechanisms and magma source regions. J Geophys Res 102:10909–10931. doi:10.1029/97JE00717

Yingst RA, Head JW (1999) Geology of mare deposits in South Pole–Aitken Basin as seen by Clementine UVVIS data. J Geophys Res 104:18957–18979. doi:10.1029/1999JE900016